Magnetic-thermal analysis of distribution transformer

Validation via optical fiber sensors and thermography

Abdali, Ali; Abedi, Ali; Maoumkhani, Hossein; Mazlumi, Kazem; Rabiee, Abbas; Guerrero, Josep M.

Published in:
International Journal of Electrical Power and Energy Systems

DOI (link to publication from Publisher):
10.1016/j.ijepes.2023.109346

Publication date:
2023

Document Version
Publisher's PDF, also known as Version of record

Electrical Power and Energy Systems 153 (2023) 109346

Contents lists available at ScienceDirect

International Journal of Electrical Power and Energy Systems

journal homepage: www.elsevier.com/locate/ijepes

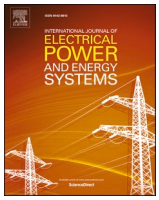

Magnetic-thermal analysis of distribution transformer: Validation via optical fiber sensors and thermography

Ali Abdali [a,b,*], Ali Abedi [c], Hossein Masoumkhani [a,d], Kazem Mazlumi [a,*], Abbas Rabiee [a], Josep M. Guerrero [e]

[a] Department of Electrical Engineering, Faculty of Engineering, University of Zanjan, Zanjan, Iran
[b] Zanjan Electricity Distribution Company (ZEDC), Zanjan, Iran
[c] Department of Mechanical Engineering, Faculty of Mechanical Engineering, Tarbiat Modares University, Tehran, Iran
[d] R&D Department, Kooshkan Transformers Company, Industrial Park No. 1, Zanjan, Iran
[e] CROM Center for Research on Microgrids, AAU Energy, Aalborg University, 9220 Aalborg, Denmark

ARTICLE INFO

Keywords:
Distribution transformer (DT)
Hotspot temperature (HST)
Nonuniform magnetic-thermal analysis
Computational fluid dynamic (CFD)
Optical fiber sensor (OFS)
Thermography

ABSTRACT

Thermal condition monitoring of distribution transformers (DTs) as the most important and expensive equipment of the power grid is undeniable, and by accurate investigation of its thermal status, its failure can be prevented because the insulation condition of the transformer is directly related to the hotspot temperature (HST). In this paper, accurate and nonuniform magnetic-thermal analysis of DT is proposed for precise HST prediction. In the magnetic analysis, the DT is modeled as a 2D axial symmetry and the losses calculation of the windings has been fulfilled as a nonuniform. In the thermal analysis, the DT is modeled as 3D and nonuniform and the conservator and core stacking, which has a considerable effect on the HST, is precisely modeled. By taking advantage of optical fiber sensors (OFSs) in the understudied 500 kVA DT the accuracy of the proposed nonuniform 3D CFD-based modeling during the temperature rise test (TRT) is validated. The empirical evaluation results depict that the presented nonuniform CFD-based thermal analysis for HST prediction is very precise and there is an appropriate vicinity to the experimental values. The error percentage of the proposed 3D CFD-based thermal analysis is 0.11 % (0.1 °C) compared to the OFSs measurements, which demonstrates the precision and effectiveness of the presented modeling. Also, the verification of the results of nonuniform 3D CFD-based thermal analysis in top-oil temperature (TOT) and bottom-oil temperature (BOT) during the experimental TRT is fulfilled via thermography. According to the attained evaluated results, temperatures of 3D CFD-based thermal analysis and thermography in the noted two points are in good accordance with each other. In short, the error percentage is less than 0.65%, which indicates the correctness and proper performance of the proposed nonuniform 3D CFD-based modeling.

1. Introduction

1.1. Background and motivation

Distribution transformers (DTs) are considered the fundamental equipment between the electricity grids and consumers, which has the role of transferring energy from the upstream network to the downstream consumers. Furthermore, due to the large number of DTs and the high cost of this equipment, their failure has a significant impact on the power quality of the energy system. Also, some failures may lead to the repair or replacement of the DT, which is not economical for distribution companies and operators.

Consequently, it is very important to monitor the DT status. For the purpose of condition monitoring of the transformers, thermal analysis is an essential step. Transformer status and thermal analysis are most affected by the hotspot temperature (HST), which is the maximum temperature of the winding. HST directly influences transformer insulation's lifetime, and every 6 °C increase in HST doubles paper insulation's aging rate, halving transformer residual useful life [1–8]. As a result, DTs' thermal behavior and HST predictions must be accurate.

* Corresponding authors.
E-mail addresses: ali_abdali@znu.ac.ir (A. Abdali), a.abedi@modares.ac.ir (A. Abedi), h.masumkhani@znu.ac.ir (H. Masoumkhani), kmazlumi@znu.ac.ir (K. Mazlumi), rabiee@znu.ac.ir (A. Rabiee), joz@energy.aau.dk (J.M. Guerrero).

https://doi.org/10.1016/j.ijepes.2023.109346
Received 12 March 2023; Received in revised form 21 May 2023; Accepted 22 June 2023
Available online 2 July 2023

Table 1
Classification and comparison of different approaches in transformer thermal analysis.

Classification and comparison of different approaches in transformer thermal analysis

Method	Complexity	Accuracy	Generality	Time	Different Loading Accuracy	Temperature Distribution	2D/ 3D Vision	Nonlinear Calculation
IEC 60076-7 & IEEE C.57.91 [1, 2]	Low	Moderate	High	Low	Moderate	×	×	×
Electro-Thermal Resistance Model (E-TRM) [9- 18]	Moderate	Moderate	Moderate	Low	Moderate	×	×	✓
AI-Based [19- 24]	Moderate	Moderate	Moderate	Moderate	Moderate	×	×	×
CFD-Based [25- 30]	High	High	Moderate	High	High	✓	✓	✓

1.2. Literature review

Several methods have been presented in the well-known literature for HST prediction. It is widely agreed that the thermal analysis behavior of transformers is commonly categorized into four comprehensive approaches. These four comprehensive methods include (1) formula-based or analytical method, (2) electro-thermal resistance model (E-TRM) method, (3) computational fluid dynamic (CFD) method, and (4) artificial intelligence (AI)-based method. But due to the fact that the proposed method in this paper is based on CFD, the literature review studies have been categorized into general non-CFD-based and CFD-based methods.

1.2.1. Non-CFD methods

A thermal model including mathematical formulas for the HST calculation and the insulation relative aging rate was presented in IEC 60076–7 [1]. For HST prediction, IEC 60076–7 presents exponential and differential formulas. According to the exponential formulas, the sum of the ambient temperature, the top-oil temperature rise (TOT), and the gradient of HST to TOT is equal to HST. In the differential approach, the feedforward block diagram was utilized for HST calculation. This approach is appropriate for online monitoring and has no limitations on the load profile and ambient temperature.

The IEEE C57.91 has tried to predict HST by taking advantage of simple formulas. Despite not considering the transformer windings and heat transfer concepts, the accuracy of prediction of the HST via the IEEE C57.91 is fairly appropriate in the steady state but does not provide proper precision for the prediction of the HST in the transient mode [2].

In [3], the authors proposed the analytical method for HST and the different points temperature distribution prediction of the DT based on a closed-form mathematical approach via a generalized heat conduction model. In this study, the nonuniformity of the different parts of the winding and the incorporation of distributed heat sources have been considered. Due to the fact that the proposed method has not been validated with experimental tests, no information is available about the accuracy of the proposed method.

E-TRM is one of the highly-recognized and trustworthy approaches for the transformer's thermal analysis. In this approach, the thermal resistance is considered for each heat flow path, and at the end, a resistance equivalent circuit is formed for the entire transformer. In this method, the theory and concept of heat transfer and conduction, convection, and radiation heat transfer coefficients are used. Several thermal resistance equivalent circuits have been presented in the literature according to different transformer structures. Using the E-TRM method, it is not possible to predict the value of HST, but it is possible to calculate the value of TOT with high accuracy. Another drawback of this method is that if the heat capacity capacitors of the equivalent circuit are not modeled, the transient values of TOT cannot be predicted and only the steady state value can be calculated. Also, in this method, considering that the height of the sources of heat production, including the windings and the core, is high in proportion to their distance from the tank wall, the 3D heat transfer can be modeled as a sum of three 1D heat transfers [9–18].

In the AI approach, using historical data including loading current, recording of environmental conditions, losses values, and measurement of TOT and AI methods like neural networks, fuzzy logic, metaheuristic algorithms, support vector regression machines, and data granulation and clustering, a thermal equivalent circuit is extracted to predict HST, and an attempt is made to match the output results of the model with the experimental measurement results [19–24]. The proper prediction of HST in overloading and the effectiveness of this method in online monitoring are among the advantages of this method.

1.2.2. CFD method

Improving computer systems and increasing their computational power has made CFD one of the most widely used tools for engineering calculations and simulations in the field of fluids. In a CFD simulation, various fluid parameters such as velocity, pressure, temperature, density, and viscosity are investigated.

One of the main challenges in the simulation of the fluid flow using CFD is the validation of the obtained results, which depends on the overall structure of the simulation process. In fact, validation of the used mathematical model is very important in the simulation of the problem. Next to the mathematical model, the right choice of the numerical method is very important in the problem-solving process. In this approach, using CFD-based software packages and the finite element method (FEM), thermal analysis of the transformer and prediction of HST can be performed. Among the advantages of this method are high accuracy in HST prediction, 2D and 3D vision, display of temperature distribution in different points and oil velocity vectors, and time-consuming calculations and complex structure of implementation are among the drawbacks of this method [25–30]. Besides, because of the specific geometry of the transformer, including the conservator, the tank corrugated walls, and the core stacking, an accurate and nonuniform CFD-based modeling approach has not been presented so far. Also, the heat flux distribution in the windings was assumed to be uniform in previous studies, which is incorrect and caused the HST prediction results to be inaccurate.

The classification and comparison of different approaches in transformer thermal analysis are summarized in Table 1. ***Green*** cells in Table 1 represent the best performance and ***Red*** cells represent the worst performance among the 4 mentioned approaches.

1.3. Contributionssssss

For the thermal analysis of the DT, its produced losses by the

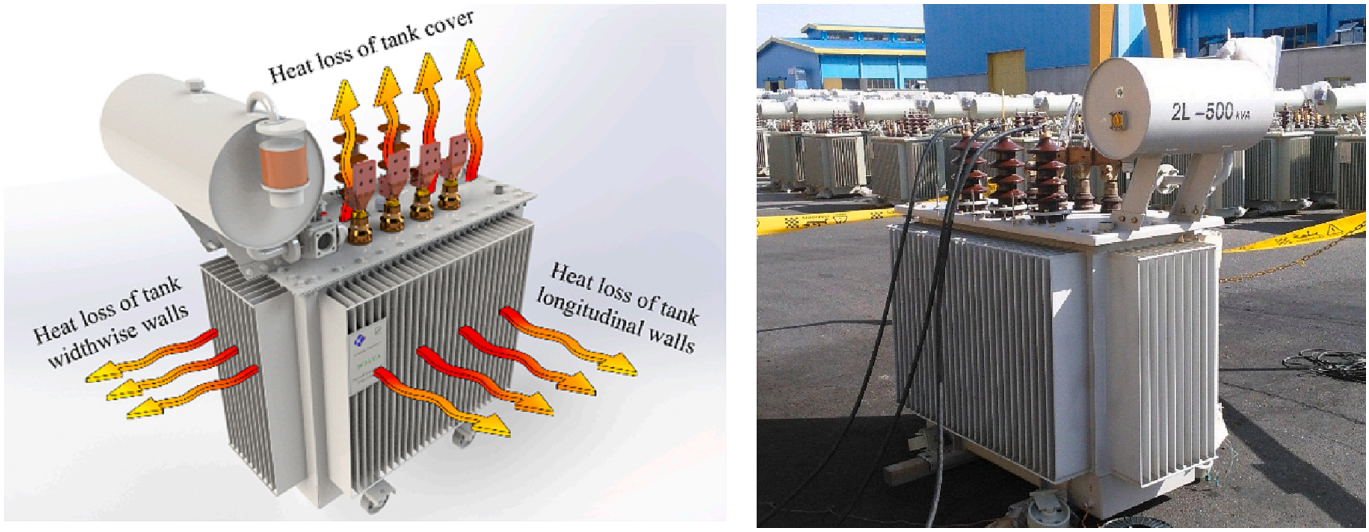

Fig. 1. The understudied 500 kVA DT.

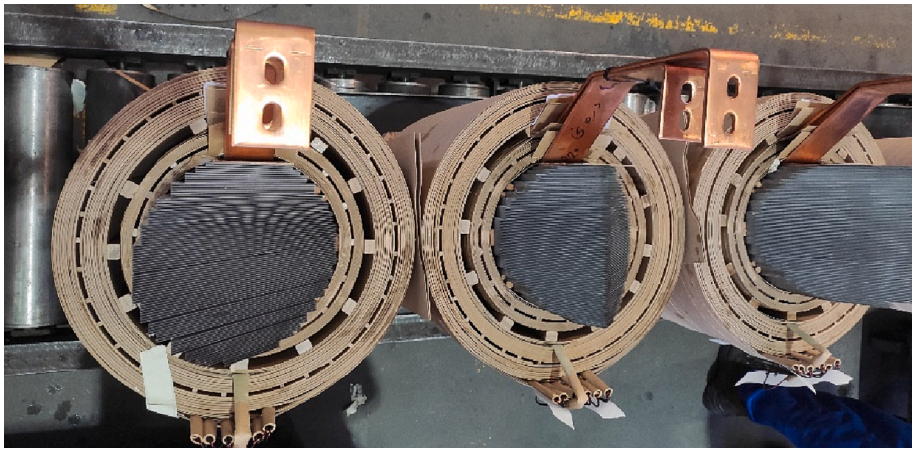

Fig. 2. 3D view of core, windings and OCs in actual DT.

windings and the core should be calculated. In previous studies, the losses have been applied through magnetic analysis or laboratory experimental results as a uniform input in thermal analysis. The assumption of uniformity of losses along the height of the windings causes the estimation of the value and location of HST to be accompanied by errors. While the windings losses are not uniform along the height, especially in the foil conductor. In this paper, the DT windings are divided into 6 segments, and in a repetition process with magnetic-thermal analysis, the ratio of each of the 6 segments of the windings in the total losses is obtained, and that losses ratio is used as an input in the thermal analysis to predict the value and location of the HST with high accuracy.

As a result, the main difference between this work and [29] is that in this paper, the heat flux distribution in the windings is considered nonuniform, and the magnetic and thermal analysis is performed using the nonuniform and converged repetition method, which has caused an increase in the accuracy of HST, TOT and bottom-oil temperature (BOT) prediction.

According to the above discussion, in this paper, accurate, nonuniform, and nonlinear magnetic-thermal analysis of DT is proposed for precise HST prediction. The conservator, which is crucial for transformer cooling, is fully and precisely modeled in this analysis since it has a significant impact on the HST. As part of the HST calculation, all DT active parts are precisely modeled, including core stacking, LV, and HV windings. It has also been demonstrated that optical fiber sensors (OFSs) and thermography are reliable measurement devices [31–33], which have been used to validate the 3D CFD-based simulation and temperature distribution and the HST value obtained from the CFD model in empirical temperature rise testing (TRT).

Hence, the main contributions of this work are summarized as follows.

- Accurate, nonuniform, and segmented magnetic analysis of DT for losses ratio calculation via 2D axial symmetry
- Accurate, nonuniform, and segmented 3D CFD-based thermal analysis of DT
- Simulation implementation as a nonuniform and converged repetition method
- Implementation of reliable experimental and industrial measurement tools including:

(i) OFSs to validate the proposed 3D CFD-based thermal analysis for HST prediction

(ii) Thermography to validate the proposed 3D CFD-based thermal analysis for TOT, and BOT prediction

2. Understudied DT

500 kVA DT is selected as the understudy transformer in this paper

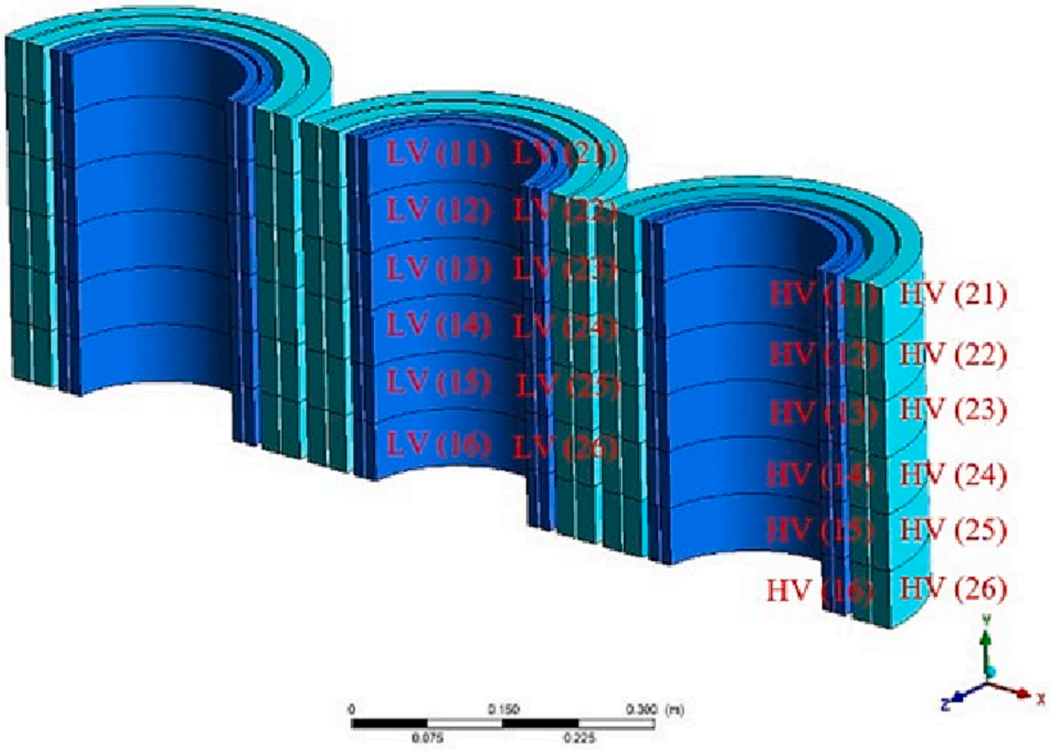

Fig. 3. 3D view of core, windings and OCs in actual DT.

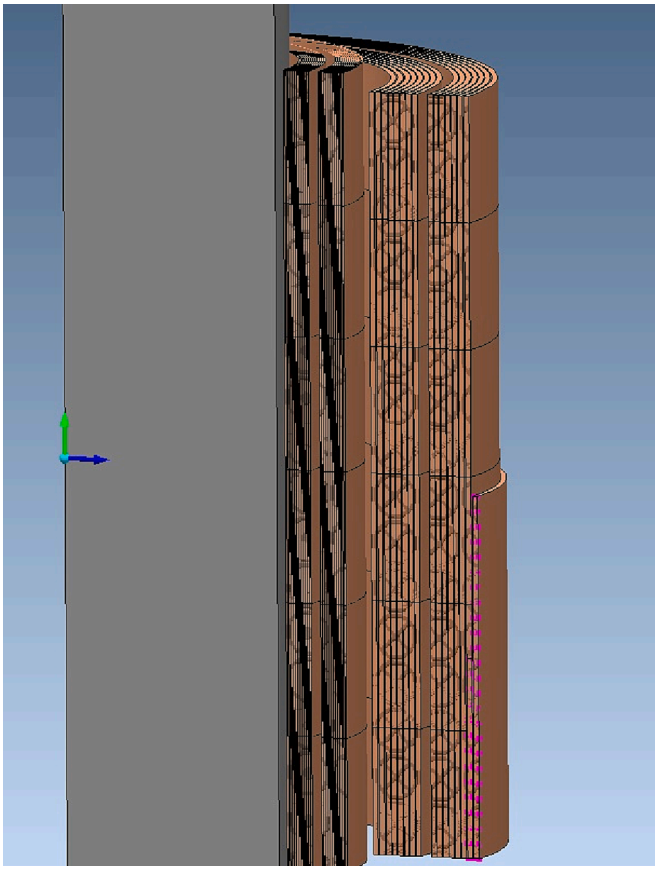

Fig. 4. 2D axial symmetry view of studied DT in MagNet Infolytica software.

that was produced by Kooshkan Transformers Company in 2022. The understudied DT contains active parts (LV and HV windings and the core), also mineral oil (MO) as the cooling fluid, cooling oil canals (OCs), conservator, and tank corrugated walls. The actual geometry of this DT tank is demonstrated in Fig. 1.

Furthermore, the detailed specifications of the DT containing dimensions of the core, HV and LV windings, HV and LV oil canals (OCs), tank, corrugated walls, and conservator are given in Table A in Appendix. As well as, the detailed cross-section modeling of the core and the windings and the OCs of windings is depicted in Fig. 2.

3. Nonuniform Magnetic-Thermal analysis of DT

3.1. Nonuniform magnetic analysis

In this section, considerations and measures taken for nonuniform magnetic analysis are mentioned. Specifically in this section, the measures and required points for magnetic analysis, including the proposed nonuniform geometry modeling, the proposed meshing to reduce the simulation time, and the governing equations of the magnetic analysis and its solution are presented.

3.1.1. Geometry modeling

For nonuniform magnetic analysis, LV and HV windings are divided into 6 segments along the height according to Fig. 3. In the studied 500 kVA DT, each of the LV and HV windings has 2 layers, and each layer is divided into 6 segments, and named as Fig. 3.

In this paper, magnetic analysis is fulfilled by MagNet Infolytica software. The geometry modeling created for magnetic analysis is shown in Fig. 4. As can be seen, the created geometry is in the form of 2D axial symmetry, and all the layers are accurately modeled with real dimensions. In this DT, the LV conductor is foil copper and the HV conductor is in the form of a round wire. In the modeling of the foil conductor, the foil conductor is modeled as solid and the round wire conductor is modeled as stranded.

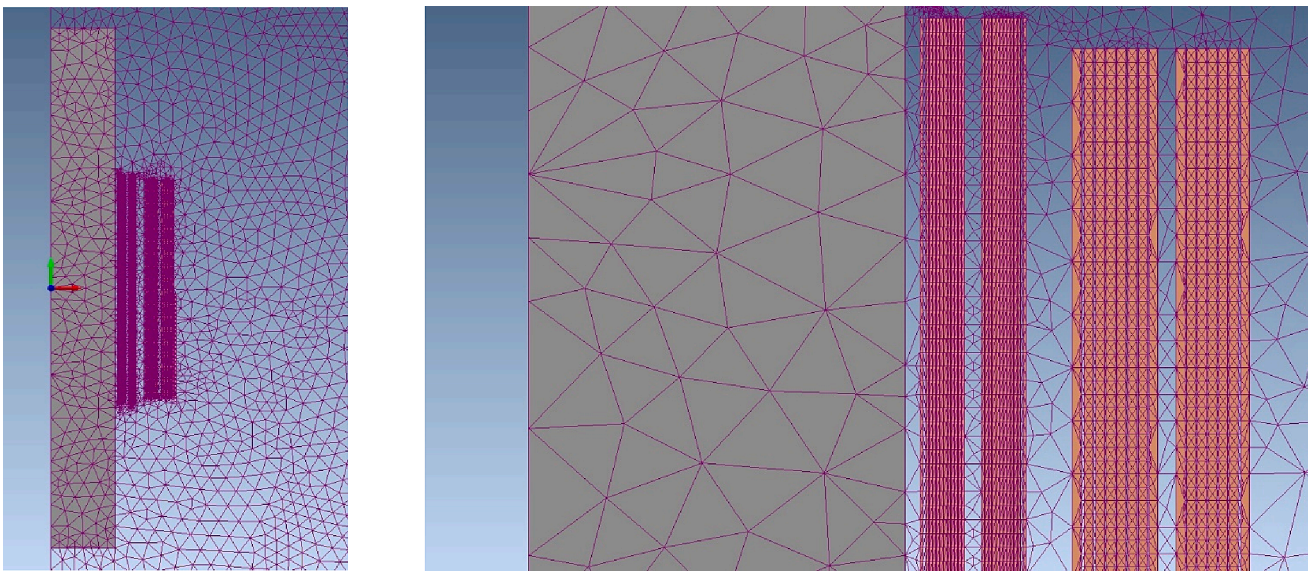

Fig. 5. Applied mesh of windings in 2D axial symmetry view of studied DT for losses calculation.

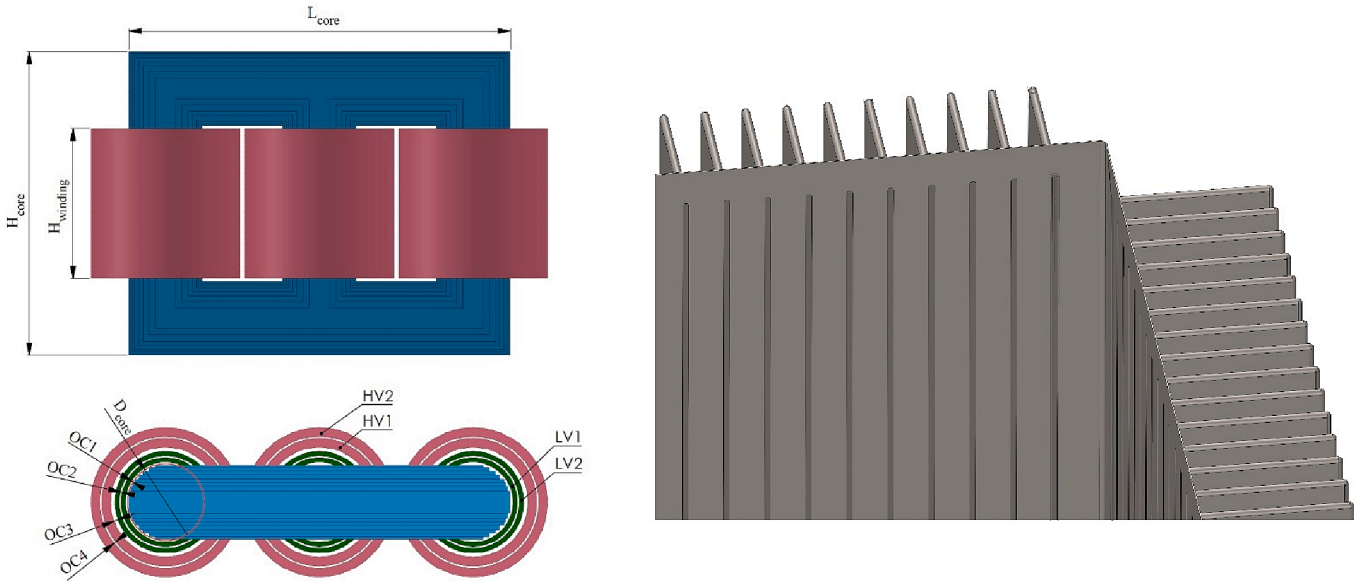

Fig. 6. Simulated geometry of studied 500 kVA DT including active part (core, windings and OCs), tank and corrugated walls in Ansys Fluent software.

3.1.2. Mesh

In magnetic analysis, only the mesh size of the winding conductors is important for calculating the losses and it affects the accuracy of the results. As a result, the mesh size of the core, the distances between layers, and the surrounding environment have no effect on the accuracy of the results. In this paper, the minimum element size of mesh for conductors is considered to be 0.5 mm, and according to Fig. 5, the conductor mesh is considered to be a uniform triangle in order to not only have high accuracy but also to reduce the solution time.

3.1.3. Governing equations

In order to calculate the time-varying magnetic field, MagNet Infolytica analyzed the eddy currents utilizing an Eddy-current solver, allowing the analysis of time-harmonic eddy currents. There are two types of losses in a transformer: core losses and winding losses (Ohmic). In terms of transformer parameters, the transformer manufacturer provides information about a transformer's primary and secondary winding current amplitudes. As a result, it is easy to use well-known harmonic current source models both in the primary and secondary windings. Using the Joule–Lenz law, the loss of power in copper windings is calculated as (1):

$$P = I_{RMS}^2 . \mathbb{R}(\bar{Z}) \tag{1}$$

Where I_{RMS} represents the root mean square of the current flowing through a winding, $\mathbb{R}(\bar{Z})$ represents the winding impedance real part, which can be determined by (2):

$$\mathbb{R}(\bar{Z}) = \frac{l}{\sigma . S} \tag{2}$$

where l represents the length of a wire used to wound a winding, S represents the cross-sectional area of a wire, and σ is electric conductivity.

3.1.4. Solution

After applying the appropriate geometry model and mesh solution,

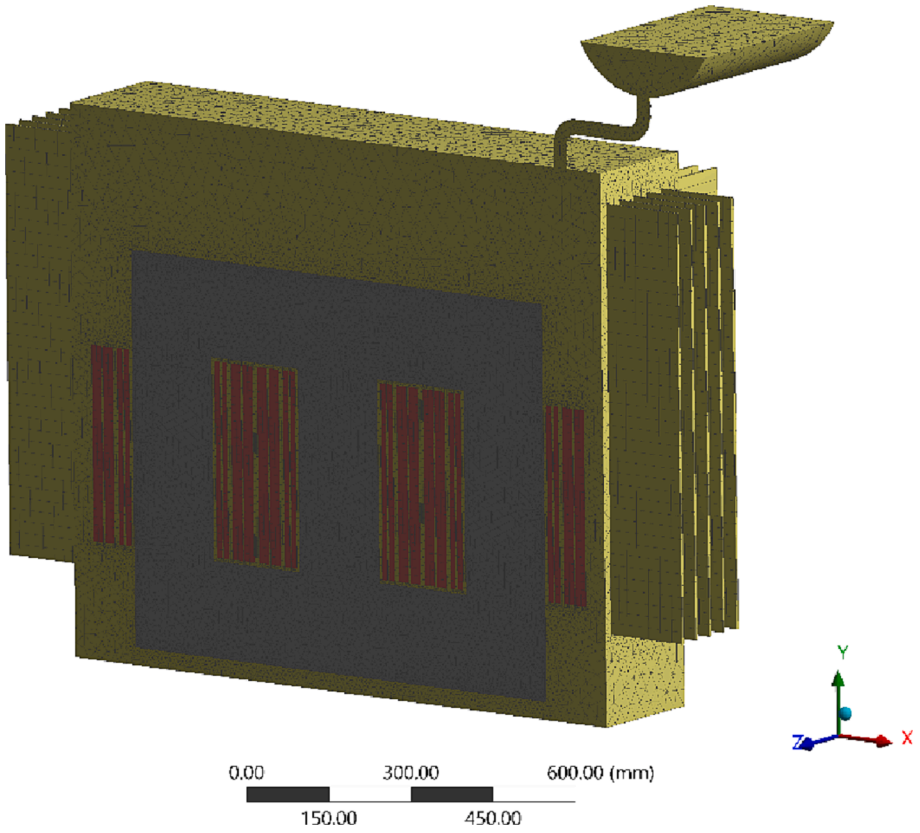

Fig. 7. Selected meth configuration in simulated geometry of the studied DT in Ansys Fluent.

the following steps are taken to calculate losses. These actions are for the calculation of the LV losses:

An AC source is applied to LV winding. The HV side is short-circuited and has zero voltage (short circuit test). A rated current is applied to the LV winding. The foil winding is selected as solid type and the round wire winding is selected as stranded with the number of turns and cross-section of each round wire. The problem is solved by the 2D Time-Harmonic method. The amount of obtained losses is the losses of LV winding at 20 °C. To obtain the total losses of the LV winding at the reference temperature of 75 °C (determined according to IEC 60076–1), (3) is used.

$$P_k(LV) = \frac{P_{20}.N_{ph}.\frac{235+75}{235+20}}{1000} = \frac{1.2157 \times 3 \times P_{20}}{1000}(kW) \quad (3)$$

where P_{20} represents loading losses obtained at 20 °C, N_{ph} represents the number of transformer phases, which is 3 for the studied DT, and the phrase $\frac{235+75}{235+20}$ is the losses conversion factor from 20C to 75C, which is the losses guarantee criterion according to the IEC 60076–1.

3.2. Nonuniform thermal analysis

In this section, considerations and measures taken for 3D CFD-based thermal analysis are mentioned. Specifically in this section, the measures and required points for thermal analysis, including the proposed nonuniform geometry modeling, types of proposed meshing for different parts of the transformer for its convergence and grid independence, governing equations of thermal analysis including thermophysical properties of different materials, governing boundary conditions of the convection and radiation heat transfer are presented.

3.2.1. Geometry modeling

This paper analyses and simulates the actual DT as a 3D model and divides the LV and HV windings into six segments along the height for non-uniform thermal analysis. Fig. 6 shows a simulated geometry for the 500 kVA DT tank, windings, core, and oil canals (OCs) of windings. Moreover, In Appendix, Table A contains specific details, specifications, and models for the DT, including the tank dimension, corrugated walls, core, conservator, LV and HV windings, and LV and HV OCs. Additionally, the winding sections are precisely modeled instead of being integrated and approximated in the modeling. Due to the symmetry in the geometry of transformers, for simplicity of modeling and analysis, transformers with conservator can be modeled as half as perpendicular to the width wall and in line with the longitudinal wall [25,28,29]. This action is common in solving CFD problems. With this action and by determining the appropriate boundary conditions along the longitudinal wall, not only the accuracy of the results does not change, but also the speed of the solving problem is doubled. It should be noted that for HST prediction, Ansys Fluent software is used to model and simulate the thermal analysis in 3D.

3.2.2. Mesh

Various sections and partitions are simulated with triangle and square mesh combinations. Denser tetrahedral meshes and smaller sizes are used where a higher degree of mesh precision is needed. Additionally, the corrugated walls have uniform square mesh. In the chosen mesh configuration, there are 712,771 elements and 2,646,314 nodes. Fig. 7 shows how the mesh is configured for the simulated DT. According to this mesh, the average orthogonal quality is 0.735, which confirms the robustness of the results.

3.2.3. Governing equations

The transformer includes different materials such as copper, paper, oil, and the thermophysical properties of these materials are different. Also, the transformer tank is considered a boundary condition where the heat transfer is different from each side. Governing equations of the transformer's materials and boundary conditions are given in Table 2

Table 2
Governing equations of the transformer's materials and boundary conditions.

Governing equations of the transformer's materials and boundary conditions

Item	Governing Equations		Descriptions
Oil	Thermophysical properties	$\rho(T) = 1098.72 - 0.712\,T$ $k(T) = 0.1509 - 7.101 \times 10^{-5}\,T$ $c_p(T) = 807.163 + 3.58\,T$ $\mu(T) = 0.08467 - 0.0004\,T + 5 \times 10^{-7}\,T^2$ $\beta(T) = 7.4 \times 10^{-4}$	It is necessary to consider the nonlinearity and temperature dependence of mineral oil (MO) thermophysical properties, which are often overlooked in existing research. This MO possesses properties such as thermal conductivity (k), density (ρ), dynamic viscosity (μ), and specific heat capacity (c_p) as a function of temperature can be determined using the following equations [9, 16].
	Continuity, momentum and energy	$\frac{\partial(\rho u)}{\partial x} + \frac{\partial(\rho v)}{\partial y} + \frac{\partial(\rho w)}{\partial z} = 0$ $\frac{\partial(\rho u^2)}{\partial x} + \frac{\partial(\rho uv)}{\partial y} + \frac{\partial(\rho uw)}{\partial z} = -\frac{\partial P}{\partial x} + \frac{\partial}{\partial x}\left(\mu\frac{\partial u}{\partial x}\right) + \frac{\partial}{\partial y}\left(\mu\frac{\partial u}{\partial y}\right) + \frac{\partial}{\partial z}\left(\mu\frac{\partial u}{\partial z}\right)$ $\frac{\partial(\rho uv)}{\partial x} + \frac{\partial(\rho v^2)}{\partial y} + \frac{\partial(\rho vw)}{\partial z} = -\frac{\partial P}{\partial y} + \frac{\partial}{\partial x}\left(\mu\frac{\partial v}{\partial x}\right) + \frac{\partial}{\partial y}\left(\mu\frac{\partial v}{\partial y}\right) + \frac{\partial}{\partial z}\left(\mu\frac{\partial v}{\partial z}\right) - \rho g$ $\frac{\partial(\rho uw)}{\partial x} + \frac{\partial(\rho vw)}{\partial y} + \frac{\partial(\rho w^2)}{\partial z} = -\frac{\partial P}{\partial z} + \frac{\partial}{\partial x}\left(\mu\frac{\partial w}{\partial x}\right) + \frac{\partial}{\partial y}\left(\mu\frac{\partial w}{\partial y}\right) + \frac{\partial}{\partial z}\left(\mu\frac{\partial w}{\partial z}\right)$ $\frac{\partial(\rho C_p uT)}{\partial x} + \frac{\partial(\rho C_p vT)}{\partial y} + \frac{\partial(\rho C_p vT)}{\partial z} = \frac{\partial}{\partial x}\left(k\frac{\partial T}{\partial x}\right) + \frac{\partial}{\partial y}\left(k\frac{\partial T}{\partial y}\right) + \frac{\partial}{\partial z}\left(k\frac{\partial T}{\partial z}\right)$	Continuity, momentum, and energy are governing equations in CFD-based MO models. The continuity equation is represented by the first equation. The second, third, and fourth equations belong to momentum equations for the x, y, and z axes. The last equation relates to the conservation of energy.
Windings	Thermal properties of the copper and insulation paper **Copper**: ρ = 8900 kg.m⁻³, C_p = 385 j.kg⁻¹.k⁻¹, k = 401 w.m⁻¹.k⁻¹ **Insulation Paper**: ρ = 930 kg.m⁻³, C_p = 1340 j.kg⁻¹.k⁻¹, k = 0.19 w.m⁻¹.k⁻¹ $pr = \frac{m_{cu} \times pr_{cu} + m_{paper} \times pr_{paper}}{m_{cu} + m_{paper}}$ Thermophysical properties of the windings **LV**: m_{paper} = 4.5 kg, m_{cu} = 110.1 kg, $m_{winding}$ = 114.6 kg, $\rho_{winding}$ = 6554 kg.m⁻³, $C_{winding}$ = 422.5 j.kg⁻¹.k⁻¹, $k_{winding}$ = 385.2 w.m⁻¹.k⁻¹ **HV**: m_{paper} = 24 kg, m_{cu} = 203.8 kg, $m_{winding}$ = 227.8 kg, $\rho_{winding}$ = 4716 kg.m⁻³, $C_{winding}$ = 485.5 j.kg⁻¹.k⁻¹, $k_{winding}$ = 358.7 w.m⁻¹.k⁻¹		Copper and insulation paper are used to produce transformer windings. c_p represents specific heat, ρ represents density, and k represents thermal conductivity. The new thermophysical properties (pr) of HV and LV windings are calculated based on the weights of the insulation paper and copper. As a matter of fact, copper and insulation paper make up the windings' thermophysical properties.
Magnetic-Thermal Analysis of Distribution Transformers			
Air	Air properties at the standard pressure of 1 atm **25 °C**: β = 0.0033 K⁻¹, ν = 1.585 × 10⁻⁵ m².s⁻¹, α = 2.174 × 10⁻⁵ m².s⁻¹, k = 0.02570 w.m⁻¹.k⁻¹		The thermophysical properties of the air at 25 °C ambient are given.
Boundary Conditions	Studied DT boundary conditions with the ambient air at temperature of T∞ =25 °C **Cover (Lid)**: $Nu = 0.54Ra^{\frac{1}{4}}$, $10^4 < Ra_L < 10^7$, h= 5.6 **Horizontal face-down (bottom)**: $Nu = 0.27Ra^{\frac{1}{4}}$, $10^5 < Ra_L < 10^{10}$, h= 2.8 **Corrugated walls**: $Nu = 0.59Ra^{\frac{1}{4}}$, $Ra_y = \frac{g\beta(T_w - T_a)y^3}{\nu\alpha}$, h= 4.2 **Conservator**: $Nu = \left\{0.6 + \frac{0.387 \times Ra^{\frac{1}{6}}}{\left(1 + \left(\frac{0.559}{P_r}\right)^{\frac{9}{16}}\right)^{\frac{8}{27}}}\right\}^2$, $10^5 < Ra_y < 10^{13}$, h= 5.2 $R_{rad} = \frac{1}{h_{rad}A}$ $h_{rad} = \varepsilon\sigma(T_s + T_a)(T_s^2 + T_a^2)$		For HV and LV windings, as well as the core, under the nominal operating conditions of the DT, the generated heat is 54868 W/m3, 152124 W/m3, and 10763 W/m3, respectively. The connector tube to the conservator has an inner diameter of 33mm and a height of 325mm. Due to the established equation $\frac{D}{H} > Ra_H^{\frac{-1}{4}}$, the equations pertaining to the constant flux for the vertical wall are applied to this tube; Surface curvature plays no effective role on lateral surfaces. By comparing the average temperature in the tube with the ambient air temperature at distance y, the local Rayleigh number can be calculated. Using equations related to the horizontal cylinder, the longitudinal wall of the conservator was studied. There are many similarities between these equations and those related to convection adjacent to a vertical wall. Vertical plane equations are used for planes surrounding the conservator. Using the boundary condition, thicknesses can be defined for the tank and other sections, such as the cover (lid), in order to surround the oil with a steel shell of the given thickness. P_r, Ra, and Nu are Prandtl, Rayleigh, and Nusselt numbers respectively. Moreover, ν is the kinematics viscosity of oil, g is Earth's gravity acceleration, β is the coefficient of volume expansion of oil, α is the thermal diffusivity of oil, y is the characteristic length, and T_w and T_a are respectively surface and ambient temperatures. Heat is transferred via radiation to the surrounding environment. There is an unlimited surface area in the environment. σ represents the Stefan-Boltzmann constant and ε represents the emissivity of the surface. A 0.9 emissivity has been applied to all other parts of the study.

along with the relevant explanations [12,25,29,34,35].

4. Results

4.1. Nonuniform Magnetic-Thermal analysis with repetition process

In this section, the results of the nonuniform magnetic-thermal analysis that was performed in a repetition process are presented. Specifically in this section, the process based on the repetition of nonuniform magnetic-thermal analysis is described, and then the loss ratio of each section is obtained, and the figures of the nonuniform current density distribution of the windings and the nonuniform temperature distribution of the windings and oil are given.

As mentioned, in previous studies, windings losses were uniformly

Table 3
Results of magnetic-thermal analysis performed in the repetition process.

Results of magnetic-thermal analysis performed in the repetition process																
	Initial		1st Iteration			2nd Iteration				3rd Iteration				Final		
Analysis	Mag.		Therm.			Mag.	Therm.			Mag.	Therm.			Mag.		Therm.
Output	Temp. (°C)	Losses (kW)	Temp. (°C)	Diff. (°C)	Diff. (%)	Losses (kW)	Temp. (°C)	Diff. (°C)	Diff. (%)	Losses (kW)	Temp. (°C)	Diff. (°C)	Diff. (%)	Losses (kW)	Ratio (%)	Temp. (°C)
LV (11)	50	0.309	84.6	34.6	40.9	0.334	85.2	0.6	0.7	0.335	85.2	0.0	0.0	0.335	**13.15**	87.1
LV (12)	50	0.127	84.1	34.1	40.5	0.143	84.6	0.5	0.6	0.143	84.6	0.0	0.0	0.143	**5.61**	86.4
LV (13)	50	0.133	83.3	33.3	40.0	0.151	83.8	0.5	0.6	0.151	83.8	0.0	0.0	0.151	**5.92**	85.5
LV (14)	50	0.132	82.7	32.7	39.6	0.149	83.2	0.4	0.5	0.149	83.2	0.0	0.0	0.149	**5.87**	84.8
LV (15)	50	0.124	82.4	32.4	39.3	0.139	82.8	0.3	0.4	0.139	82.8	0.0	0.0	0.139	**5.45**	84.4
LV (16)	50	0.296	82.5	32.5	39.4	0.318	82.8	0.3	0.4	0.318	82.8	0.0	0.0	0.318	**12.51**	84.4
LV (21)	50	0.239	86.1	36.1	41.9	0.271	87.0	0.9	1.1	0.271	87.1	0.0	0.0	0.271	**10.66**	**90.1**
LV (22)	50	0.172	86.0	36.0	41.8	0.191	86.9	0.9	1.1	0.192	86.9	0.0	0.0	0.192	**7.53**	90.0
LV (23)	50	0.193	85.6	35.6	41.6	0.214	86.4	0.9	1.0	0.214	86.4	0.0	0.0	0.214	**8.42**	89.4
LV (24)	50	0.189	85.0	35.0	41.2	0.209	85.8	0.8	0.9	0.209	85.8	0.0	0.0	0.209	**8.22**	88.7
LV (25)	50	0.159	84.5	34.5	40.8	0.177	85.2	0.7	0.8	0.177	85.2	0.0	0.0	0.177	**6.95**	88.0
LV (26)	50	0.218	84.1	34.1	40.6	0.246	84.8	0.7	0.8	0.246	84.8	0.0	0.0	0.246	**9.67**	87.5
HV (11)	50	0.199	83.6	33.6	40.2	0.223	84.2	0.6	0.7	0.223	84.3	0.1	0.1	0.223	**8.46**	87.1
HV (12)	50	0.199	83.6	33.6	40.2	0.223	84.2	0.6	0.7	0.223	84.3	0.1	0.1	0.223	**8.46**	86.2
HV (13)	50	0.199	83.5	33.5	40.1	0.223	84.0	0.5	0.6	0.223	84.1	0.1	0.1	0.223	**8.46**	86.2
HV (14)	50	0.199	83.3	33.3	40.0	0.223	83.8	0.5	0.6	0.223	83.9	0.1	0.1	0.223	**8.45**	86.0
HV (15)	50	0.199	83.1	33.1	39.8	0.222	83.5	0.5	0.6	0.223	83.6	0.1	0.1	0.223	**8.44**	85.7
HV (16)	50	0.199	82.8	32.8	39.6	0.222	83.3	0.4	0.5	0.223	83.3	0.1	0.1	0.223	**8.43**	85.4
HV (21)	50	0.203	81.2	31.2	38.4	0.225	81.6	0.4	0.5	0.226	81.6	0.0	0.0	0.226	**8.55**	85.1
HV (22)	50	0.203	81.1	31.1	38.4	0.225	81.5	0.4	0.5	0.226	81.6	0.0	0.0	0.226	**8.55**	82.8
HV (23)	50	0.203	81.0	31.0	38.3	0.225	81.4	0.4	0.5	0.225	81.4	0.0	0.0	0.225	**8.55**	82.8
HV (24)	50	0.203	80.9	30.9	38.2	0.225	81.2	0.3	0.4	0.225	81.2	0.0	0.0	0.225	**8.54**	82.6
HV (25)	50	0.186	80.6	30.6	38.0	0.206	80.9	0.3	0.4	0.206	80.9	0.0	0.0	0.206	**7.80**	82.4
HV (26)	50	0.173	80.4	30.4	37.8	0.191	80.7	0.3	0.3	0.191	80.7	0.0	0.0	0.191	**7.25**	82.1

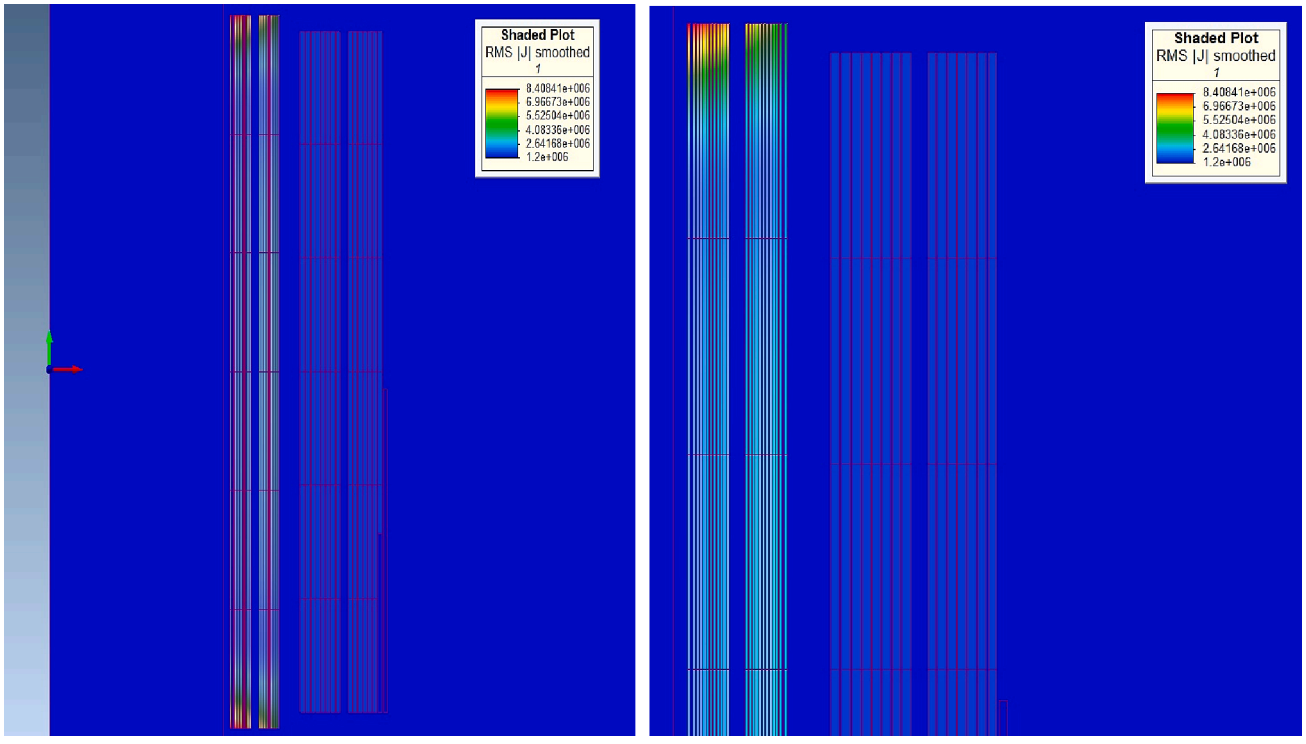

Fig. 8. Distribution of the current density of the foil conductor in the 2nd iteration of magnetic analysis.

used in thermal analysis, which caused errors in the value and location of HST. Also, these losses are obtained as input for thermal analysis from laboratory experimental tests or magnetic analysis. But investigations show that the losses, especially in foil conductors, are nonuniform along the height, and the current density and consequently the losses value are higher in some segments, which itself leads to a change in the HST value.

In this paper, LV and HV windings are modeled as 2D axial symmetry and divided into 6 segments along the height. In the initial stage, it is

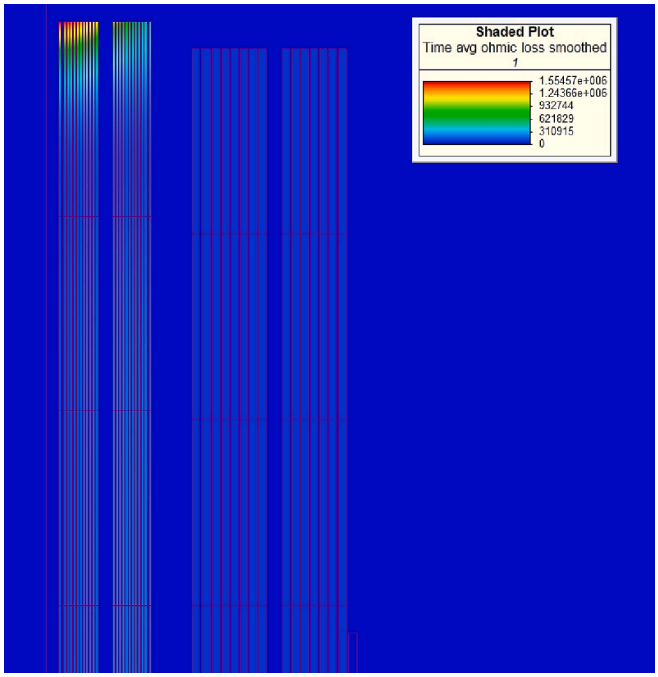

Fig. 9. Distribution of the ohmic losses of the foil conductor in the 2nd iteration of magnetic analysis.

assumed that the temperature of the LV and HV windings is 50 °C and the losses of different segments of the LV and HV windings are obtained. Then, the obtained loss values are used as input in thermal analysis and the temperature of different segments of the windings is obtained. Then, these windings' temperatures are used as input in the magnetic analysis so that the windings losses at new temperatures are obtained and used as a new input in the next iteration of the thermal analysis. This process of repetition in magnetic-thermal analysis continues until the difference in temperature changes of the windings reaches less than 0.1 °C. After obtaining the temperatures of the windings in the last iteration, these temperatures were used as a final input in the last magnetic analysis to obtain the contribution and ratio of different segments of the windings in produced losses to be used in the final thermal analysis. It should be mentioned that the amount of the final losses applied to the windings in the final thermal analysis was obtained from the experimental results of the laboratory according to the IEC 60076–1 at a reference temperature of 75 °C, and the ratio and contribution of the different segments of the windings were also done from the nonuniform magnetic-thermal analysis that is achieved from the mentioned repetition process.

The results of the magnetic-thermal analysis performed in the repetition process are shown in Table 3. As can be seen, in the 3rd iteration, the temperature difference of the windings in most segments is mostly 0 °C and in some parts 0.1 °C, which indicates that the nonuniform magnetic-thermal analysis has converged. Also, after the final magnetic and thermal analysis, the contribution and ratio of 24 segments of LV and HV windings and the final temperature of these segments have been obtained. As can be seen, the highest contribution and ratio of losses is for the LV (11) segment, and also the maximum value of HST is for the LV (21) segment and its value is equal to 90.1 °C. It can also be seen that the distribution of losses in the foil conductor is nonuniform and the distribution of losses increases in the upper, lower, and middle segments, which has a significant effect on the value and location of HST. Also, the loss distribution in the round wire conductor is nonuniform and different in the first and second layers.

The distribution of the current density of the foil conductor, the distribution of the ohmic losses of the foil conductor, and the distribution of the current density of the round wire conductor in the 2nd iteration in the short-circuited test simulation of magnetic analysis are

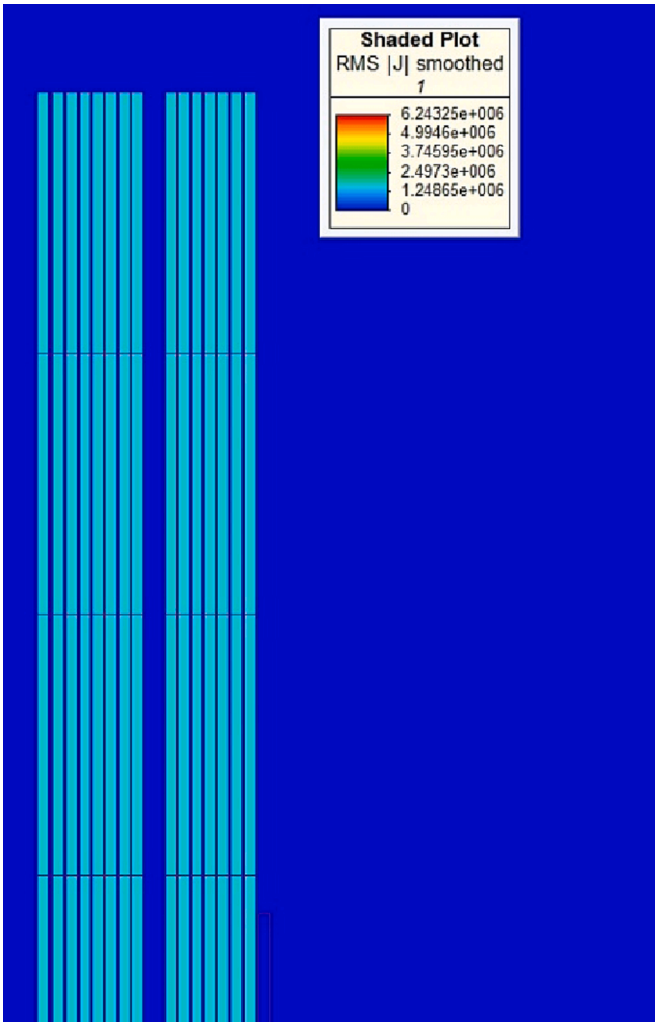

Fig. 10. Distribution of the current density of the round wire conductor in the 2nd iteration of magnetic analysis.

shown in Figs. 8 to 10, respectively.

As can be seen that the distribution of the current density and ohmic losses of the foil conductor are nonuniform and the distribution density increases in the upper, lower, and middle segments, which has a significant effect on the value and location of HST. Also, the distribution of the current density of the round wire conductor is nonuniform and different in the first and second layers.

Also, the strength of the magnetic field in the 2nd repetition in the short-circuit test when the HV side is short-circuited is shown in Fig. 11.

Also, the temperature of different segments of LV and HV windings, the temperature distribution of MO fluid, and the MO velocity vector in the final iteration of thermal analysis are shown in Figs. 12 to 14.

According to the results obtained from CFD-based thermal analysis, the maximum value of HST is for the LV (21) segment and its value is equal to 91.3 °C. As well as, the values of TOT and BOT obtained from CFD-based thermal analysis are 77.4 °C and 64.9 °C respectively.

4.2. Experimental validation via OFSs and thermography measurement

An evaluation of the proposed 3D CFD-based modeling was conducted using TRT (heat-run) according to IEC 60076–2:2011, where the numerical results were compared to those obtained from experimental laboratory tests. The DT secondary (LV winding) is short-circuited during the temperature test, and the total loss, including no-load and load losses, is taken into account. The studied DT has core losses,

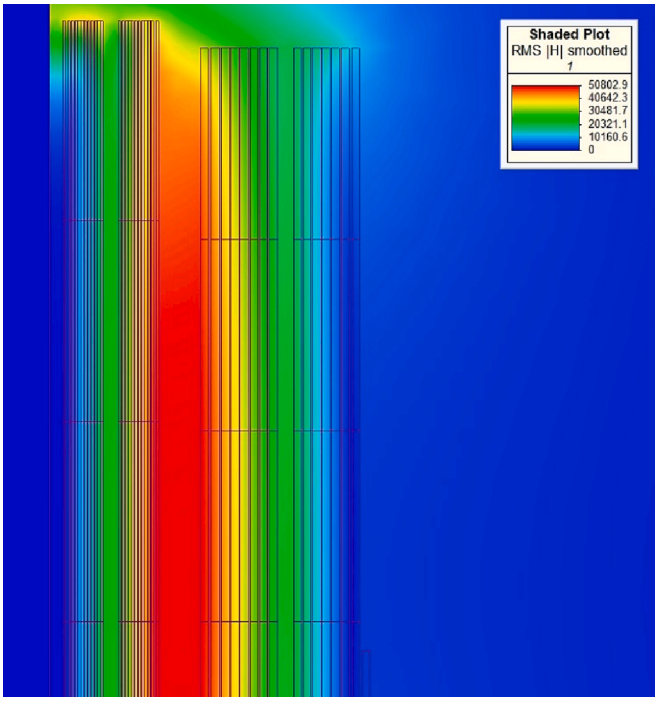

Fig. 11. Strength of the magnetic field in the 2nd repetition in the short-circuit test when the HV side is short-circuited.

winding losses, and rated tank heat disposal capacities of 0.853 kW, 5.1 kW, and 8.98 kW, respectively. In order to gain the oil temperature rise, total losses need to be applied to the DT. A steady-state oil temperature rise is established during this test by monitoring the TOT. The experimental test was carried out on a 500 kVA, 20/0.4 kV, $U_k = 6\%$ DT that was designed by the Kooshkan Transformer Company. As shown in Fig. 15, the TRT in the HV laboratory was performed in March 2022, and values were measured by thermography.

Ten OFSs are placed throughout the active parts of the studied transformer in different spots within the active parts to analyze the proposed 3D CFD-based thermal analysis.

Fig. 16 shows the view, location, and implementation of OFSs in understudied DT. Because the HST position is probabilistic, and its precise location cannot be predicted with certainty, it is generally accepted that the HST is located in the upper 20% of the windings and most often near or within the inner layer of windings (LV windings) due to high current flow [1].

In one-second intervals, the data acquisition system collects and records the temperature values of OFSs. It should be noted that the mean values of the temperature in the last minute of each interval during TRT are presented in Table 4 according to the available noise and momentary changes in the measured temperature values. A detailed description of the HST measurement results for 10 OFS in the DT during different hours of TRT is also provided in Table 4. The measurement from OFS 1 could be considered the actual HST since it has the highest measured temperature among the 10 OFSs.

Based on the proposed CFD-based non-uniform thermal analysis, the predicted HST is 90.1 °C, nearly matching their experimental value, i.e., the results of OFS 1. HST measurement results and associated errors are presented in Table 5.

By analyzing the thermal behavior of the understudied DT during the TRT with thermography, the results of non-uniform 3D CFD simulations can be verified. In order to accomplish this goal, two critical points are taken into consideration during TRT using thermography. Using thermography for these two points, if their temperature is well in agreement with the results obtained from CFD-based thermal analyses, this would indicate that the proposed non-uniform 3D CFD-based thermal analysis of the understudied DT is accurate. The BOT and TOT are the two points that are considered. Fig. 17 shows the thermography results from the BOT and TOT for the understudied DT during the TRT. Based on the results of Fig. 13 and Fig. 17, Table 6 shows the temperatures for these two points.

Table 6 shows that the outputs of the 3D CFD-based thermal analysis, thermography, and OFSs are in reasonable agreement with each other at these spots and differ by no more than 0.5 °C (less than0.65 %), which confirms that the proposed 3D CFD-based thermal model of the understudied DT can accurately predict experimental results and have high accuracy. Tables 5 and 6 demonstrate that the proposed nonuniform thermal analysis method is more accurate than the uniform method because it calculates values for HST, TOT, and BOT more accurately.

4.3. Discussion

As stated in the Introduction, the HST estimation methods are categorized into four comprehensive methods including 1) formula-based or analytical method, 2) electro-thermal resistance model (E-TRM) method, 3) computational fluid dynamic (CFD) method, and 4) artificial intelligence (AI)-based method. In this paper, the proposed method for HST prediction is based on CFD and according to magnetic-thermal analysis. In most of the studies, the heat flux distribution is considered constant, while due to the structure of the windings of DT, the heat flux distribution is not constant and is nonuniform.

In this paper, the proposed nonuniform iterative-based magnetic-

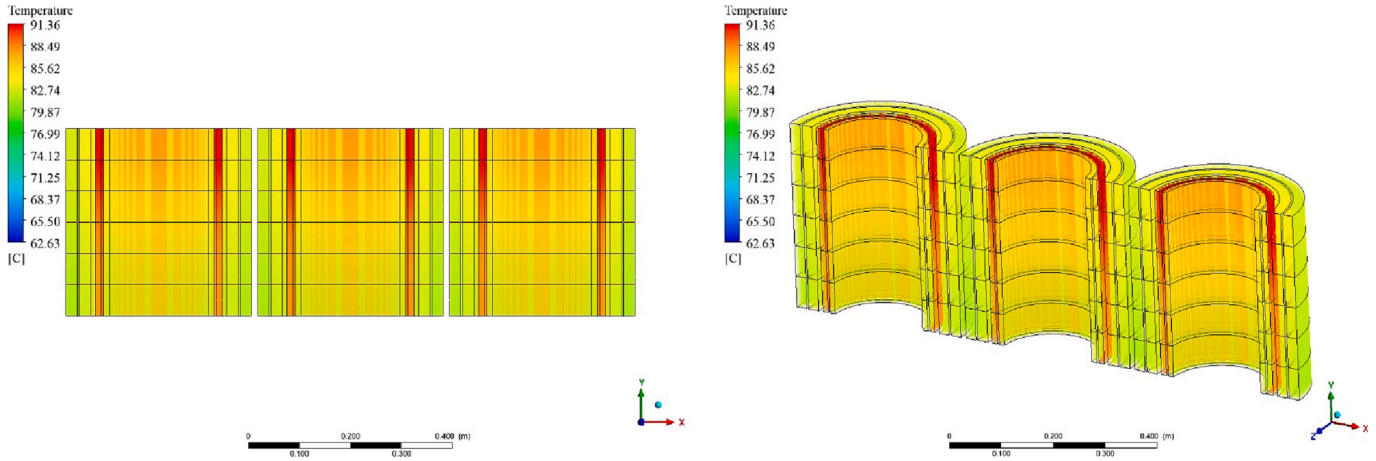

Fig. 12. 2D and 3D temperature distribution of different segments of LV and HV windings in the final iteration of thermal analysis.

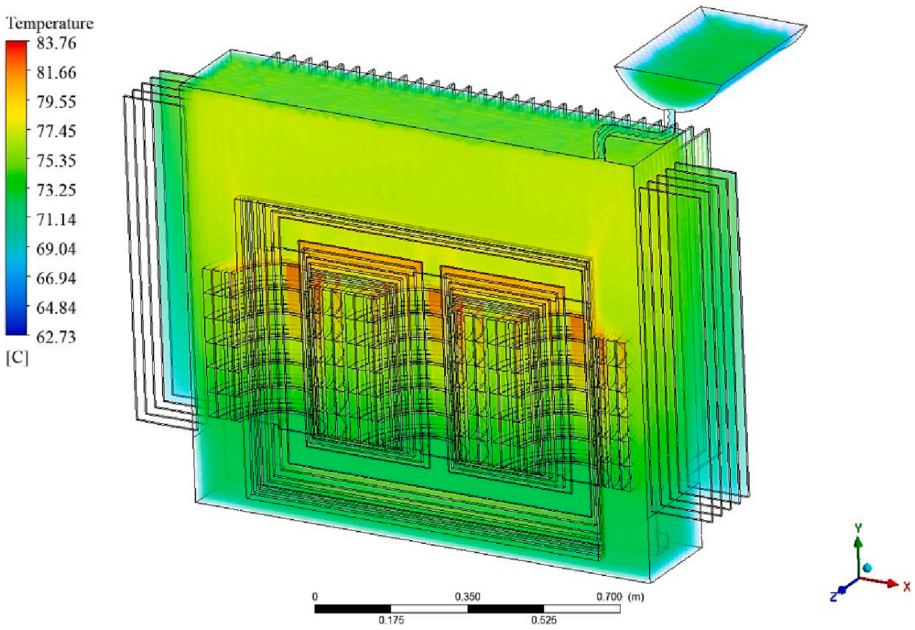

Fig. 13. Temperature distribution of MO fluid in the final iteration of thermal analysis.

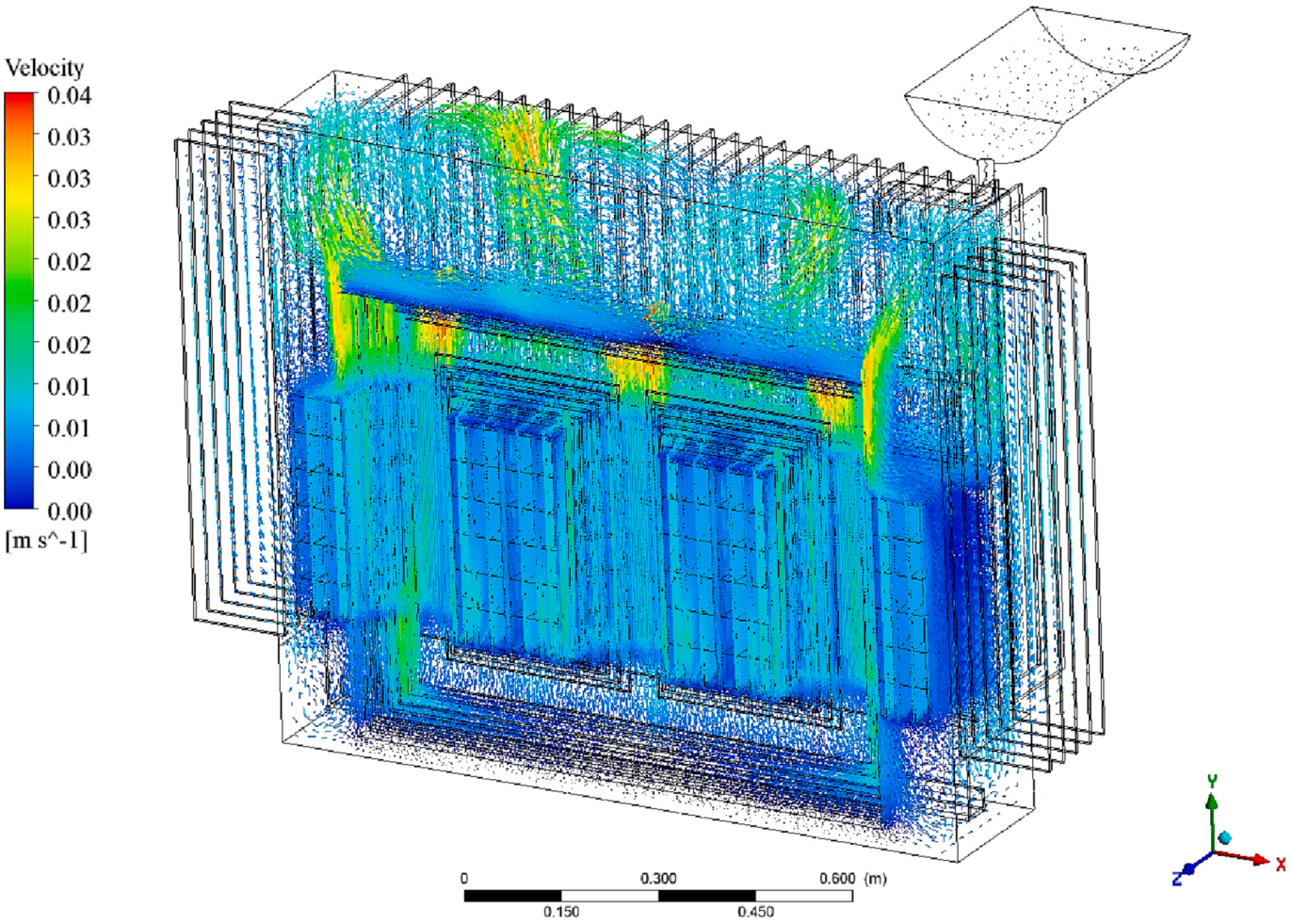

Fig. 14. MO velocity vector in the final iteration of thermal analysis.

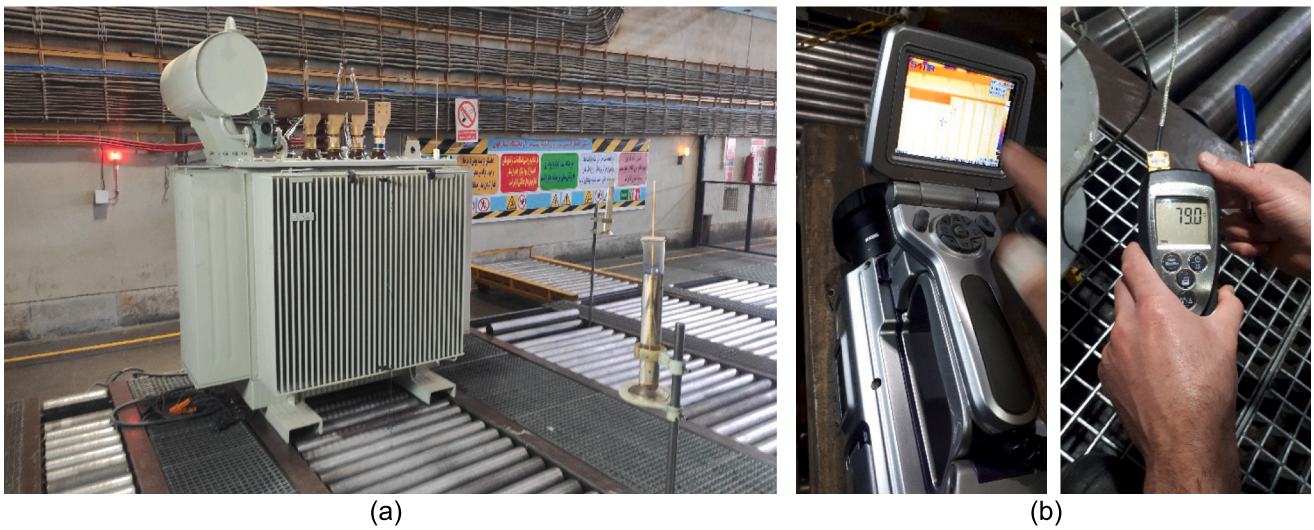

Fig. 15. (a) The studied 500 kVA DT during TRT in the HV laboratory, (b) thermography measurement of 500 kVA DT during TRT.

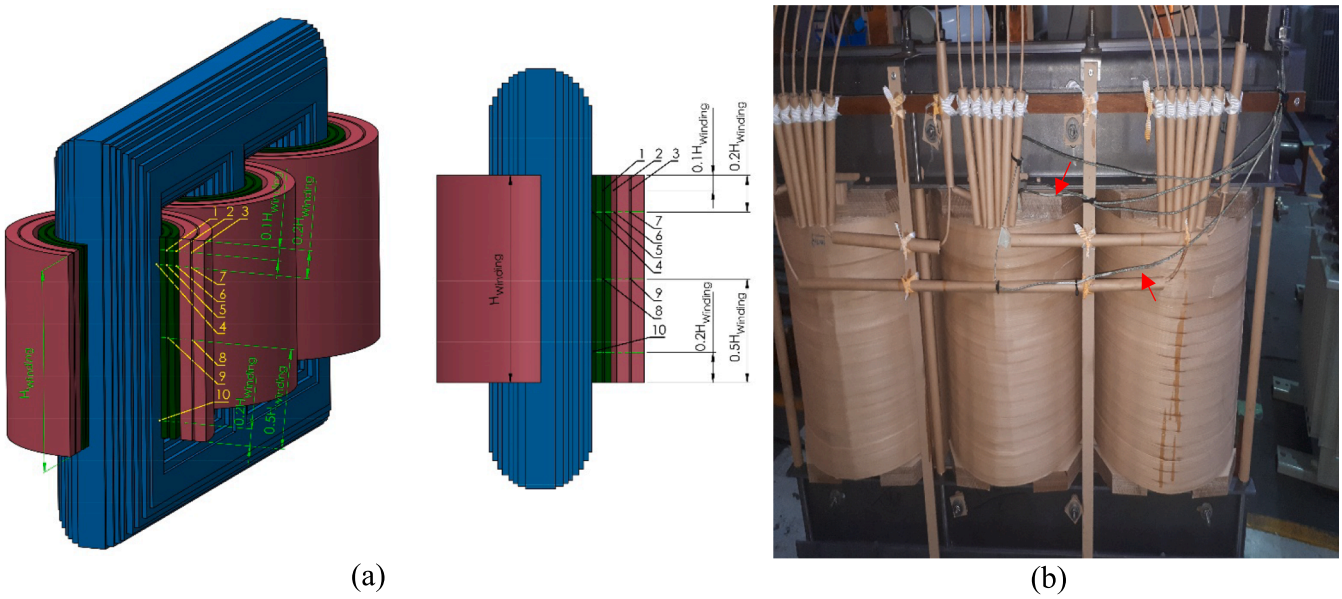

Fig. 16. (a) OFSs installation and positions in studied windings of DT, (b) Schematic diagram of OFSs positions.

thermal analysis has been performed accurately in order to estimate the HST with high accuracy. Also, industrial measurement tools such as OFS and thermography have been used in experimental TRT testing to validate the proposed method.

In this paper, HST values obtained from CFD are compared with windings temperature values measured by OFS. It should be noted that according to Figs. 16, 10 OFSs are installed in different parts of the windings to measure the instantaneous temperatures of the windings to determine the value and location of HST (Table 4).

However, the values of TOT and BOT obtained from CFD are compared with the values measured by thermography. As you mentioned, the thermography measures the temperature of the tank surface. The utilization scheme of these industrial measurement tools (OFS and thermography) in experimental validation is shown in Fig. 18.

Also, the comparison of the proposed method with the other papers mentioned in the Introduction is shown in Table 7.

According to the results of Table 7, it can be said that the proposed model is the most complete model presented among these studies and has been validated with comprehensive experimental tests. The results show that the proposed method can predict more accurately the values of HST, TOT, and BOT compared to other methods. The reason for the high accuracy of the estimation of thermal parameters is related to nonuniform magnetic-thermal analysis. Also, in the proposed thermal analysis of the DT, the conservator which is crucial for transformer cooling, is fully and precisely modeled in this analysis since it has a significant impact on the HST.

Table 8 also shows the comparison of the HST estimation results of the proposed method with the proposed formula of IEC 60076–7 and IEEE C57.91 [1,2].

According to the values in Tables 5, 6, and 8, it can be seen that the CFD-based HST value is close to the HST values measured with OFSs. Also, the TOT and BOT values of the CFD output are close to the TOT and BOT values measured by thermography and have a high agreement. As a result, the accuracy and performance of the proposed nonuniform CFD-based model is high.

Table 4
HST measured values via OFSs during TRT.

Time	Ambient (°C)	OFS 1 (°C)	OFS 2 (°C)	OFS 3 (°C)	OFS 4 (°C)	OFS 5 (°C)	OFS 6 (°C)	OFS 7 (°C)	OFS 8 (°C)	OFS 9 (°C)	OFS 10 (°C)	TOT (°C)	BOT (°C)
7:15	23.2	39.3	37.8	38.7	38.9	36.9	34.9	35.7	33.3	33.3	27.8	23.3	23.3
7:45	23.6	51.5	50.2	50.8	50.9	49.2	47.2	47.7	43.4	43.1	36.5	24.3	23.8
8:15	23.8	59.9	58.2	59.1	59.1	57.7	55.1	56.1	48.6	47.9	41.5	25.2	24.1
8:45	23.9	67.1	65.6	66.3	66.5	64.7	62.4	63.4	54.4	53.7	47.2	25.7	24.5
9:15	24.0	72.6	71.6	71.8	72.0	70.4	68.3	69.0	60.8	60.3	52.8	27.0	25.0
9:45	24.4	77.2	75.1	76.6	76.6	75.1	71.7	73.8	65.5	65.0	56.3	29.3	26.5
10:15	24.8	79.9	78.2	79.2	79.2	77.4	74.9	76.4	68.3	67.7	59.4	34.0	28.9
10:45	24.8	82.7	81.5	81.9	82.1	80.2	78.3	79.2	71.0	70.4	62.7	40.0	32.0
11:15	24.8	84.7	83.2	83.8	83.9	82.2	80.1	81.2	72.7	72.2	64.4	44.5	34.2
11:45	24.8	86.1	84.6	85.2	85.5	83.5	81.5	82.7	74.4	73.7	65.8	48.2	38.2
12:15	24.9	87.4	85.7	86.5	86.6	85.1	82.7	83.8	75.6	75.0	66.9	55.5	42.7
12:45	25.0	88.4	87.0	87.7	87.6	86.1	84.0	85.0	76.7	76.2	68.2	58.0	45.9
13:15	25.1	89.1	87.5	88.3	88.3	86.8	84.6	85.5	77.4	76.9	68.7	62.0	48.1
13:45	25.1	89.4	88.4	88.6	88.8	87.1	85.4	85.7	77.6	76.9	69.6	64.0	50.5
14:15	25.3	89.7	88.0	88.8	88.9	87.3	84.9	85.8	77.9	77.4	69.2	65.0	51.9
14:45	25.3	90.0	88.8	89.4	89.5	87.4	85.6	86.3	78.3	77.7	70.0	67.0	55.0
15:15	25.3	90.6	89.2	89.7	89.8	88.1	86.0	86.5	78.9	78.3	70.4	69.0	56.9
15:45	25.4	90.8	89.4	90.1	90.3	88.3	86.1	87.1	79.2	78.5	70.6	73.2	58.5
16:15	25.3	91.0	89.5	90.2	90.2	88.5	86.1	87.3	79.3	78.7	70.7	75.5	60.6
16:45	25.1	91.1	89.6	90.3	90.3	88.7	86.3	87.4	79.4	78.8	70.8	75.5	62.5
17:15	24.9	91.2	89.8	90.3	90.5	88.9	86.7	87.5	79.4	78.9	71.0	76.5	64.2
17:45	24.8	91.3	89.9	90.4	90.5	88.9	86.8	87.6	79.6	79.0	71.1	76.8	64.6
18:15	24.6	91.3	89.9	90.5	90.6	88.9	86.8	87.7	79.7	79.0	71.1	77.0	64.8
19:15	24.5	91.4	89.9	90.6	90.6	89.0	86.8	87.8	79.7	79.1	71.1	77.0	64.9

Table 5
HST value of studied 500 kVA DT via CFD and OFSs.

	OFS	CFD (Nonuniform)	CFD (Uniform) [29]
HST (°C)	91.4	91.3	90.7
Error Per. (%)	–	0.11	0.76

5. Conclusions

In this paper, accurate, nonuniform, and nonlinear magnetic-thermal analysis of DT is proposed for precise HST prediction. In the magnetic analysis, the DT is modeled as a 2D axial symmetry and the losses calculation of the windings has been fulfilled as a nonuniform. In the thermal analysis, the DT is modeled as 3D and nonuniform and the conservator and core stacking, which has a remarkable impact on the HST, is thoroughly modeled. As well as, the OFSs are utilized to verify the accuracy of the proposed nonuniform 3D CFD-based thermal analysis in HST prediction. Also, a thermography measurement is employed to approve the obtained results of the nonuniform 3D CFD-based thermal analysis in TOT, and BOT experimental TRT. The conclusions can be outlined as follows:

- By taking advantage of the proposed nonuniform and segmented magnetic analysis, it can be seen that the highest contribution and

Table 6
TOT and BOT values of studied 500 kVA DT via CFD and OFSs.

	Thermography	CFD (Nonuniform)	CFD (Uniform) [29]
TOT (°C)	76.9	77.4	77.9
Error Per. (%)	–	0.65	1.3
BOT (°C)	65.0	64.9	65.1
Error Per. (%)	–	0.15	0.15

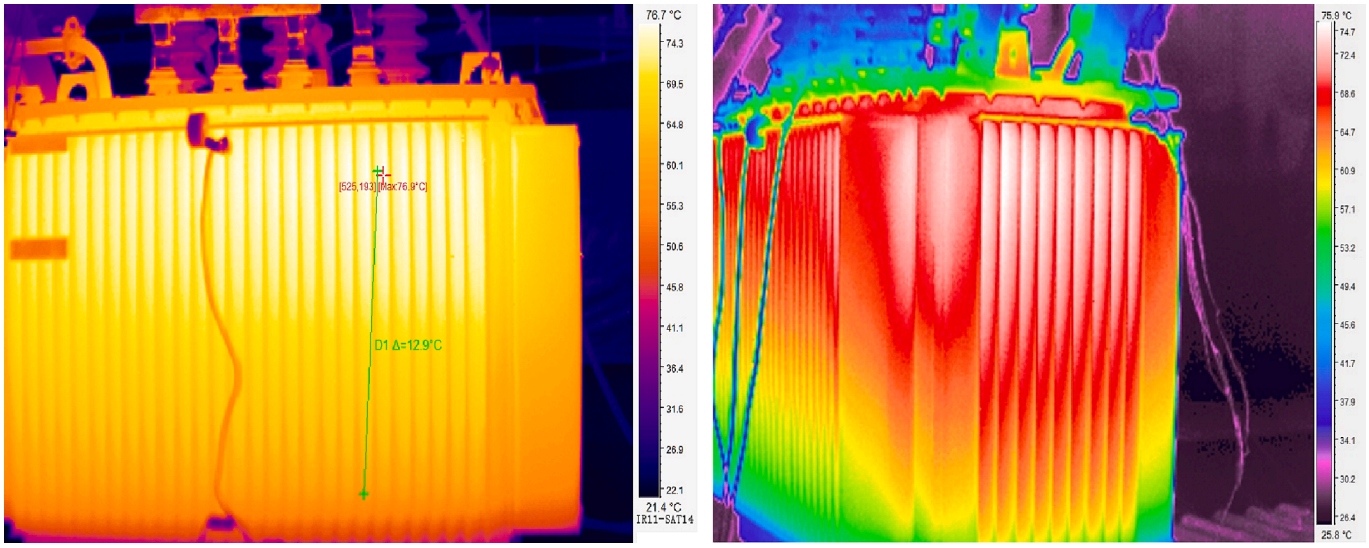

Fig. 17. TOT and BOT of studied 500 kVA DT during TRT obtained from the thermography.

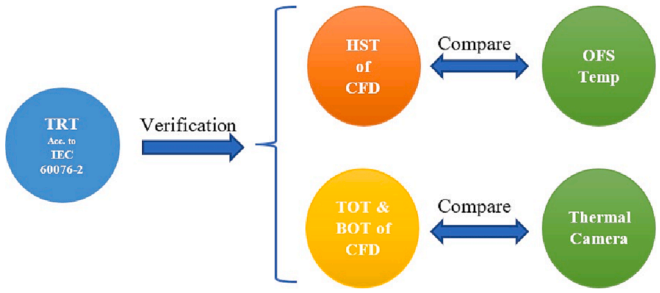

Fig. 18. Industrial measurement tools (OFS and thermography) utilization scheme in experimental validation.

ratio of losses are for the LV (11) segment. It can also be seen that the distribution of losses in the foil conductor is nonuniform and the distribution of losses increases in the upper, lower and middle segments, which has a significant effect on the value and location of HST. Also, the loss distribution in the round wire conductor is nonuniform and different in the first and second layers.

- The predicted HST value by the proposed nonuniform 3D CFD-based thermal analysis is 91.3 °C, while the measured HST value by the OFS 1 is 91.4 °C and the error percentage of 3D CFD-based thermal analysis is 0.11 % (0.1 °C) compared to OFS 1 results, which represents the precision and proficiency of the proposed nonuniform 3D CFD-based thermal analysis.
- The predicted TOT, and BOT values by the proposed nonuniform 3D CFD-based thermal analysis are 77.4 °C, and 64.9 °C respectively, while the measured TOT, and BOT values by the thermography are 76.9 °C, and 65.0 °C and the error percentage of proposed nonuniform 3D CFD-based thermal analysis are 0.65 % (0.5 °C) and 0.15 % (0.1 °C) compared to thermography measurement, which represents the precision and proficiency of the proposed nonuniform 3D CFD-based thermal analysis.
- It is possible to ensure the permissible thermal behavior of an in-service transformer by using the proposed non-uniform 3D CFD-based thermal analysis during the transformer design and experimental validation phase.

CRediT authorship contribution statement

Ali Abdali: Conceptualization, Methodology, Software, Validation, Formal analysis, Resources, Writing – original draft, Visualization, Project administration. **Ali Abedi:** Software, Validation, Formal analysis, Data curation. **Hossein Masoumkhani:** Software, Investigation, Visualization. **Kazem Mazlumi:** Validation, Data curation, Writing – review & editing, Supervision. **Abbas Rabiee:** Investigation, Data curation, Writing – review & editing, Supervision. **Josep M. Guerrero:**

Table 8
HST values comparison of studied 500 kVA DT.

	OFS	CFD (Nonuniform)	IEC 60076–7 [1]	IEEE C57.91 [2]
HST (°C)	91.4	91.3	92.2	92.4
Error Per. (%)	–	0.11	0.87	1.09

Table A1
Specifications of geometrical dimensions of studied DT.

Parameters	Value	Parameters	Value (mm)
Rate voltage (HV/LV)	20/0.4 kV	Inner diameter of LV1	194
Rate current (HV/LV)	14.4/721.7 A	Outer diameter of LV1	217
Voltage ratio	9.623 V/Turn	Inner diameter of LV2	225
Vector group	Dyn 5	Outer diameter of LV2	248
LV turns No.	24	Inner diameter of HV1	267
HV turns No. (Rated)	2078	Outer diameter of HV1	311.5
HV turns No. (Min/Max)	1974/2182	Inner diameter of HV2	319.5
Physical Parameters	**Value (mm)**	Outer diameter of HV2	364
Fin length	160	Core-LV OC1 distance	3.5
Fin thickness	8.4	LV1-LV2 OC2 width	4
Fin step distance	32	LV2-HV1 OC3 width	9.5
Fin height	800	HV1-HV2 OC4 width	4
Tank length	1212	HV distance from cover	258
Tank width	492	HV distance from lower surface	32
Tank height	1030	HV distance from longitudinal wall	58
Tank thickness	1.2	HV distance from widthwise wall	43
Cover thickness	6	Conservator length	800
Core height	739	Conservator height	640
Core diameter	187	Conservator diameter	315
Core length	930	Conservator pipe length	170
Winding's height	365	Conservator pipe diameter	33

Table 7
Comparison of different references in transformer thermal analysis: method, analysis, experimental validation, result.

References	Method	Heat Flux	Magnetic Analysis	Thermal Analysis	Thermal Parameter	Experimental Validation	Experimental Tools	Estimation Error
[3]	Analytical	Approximate Nonuniform	×	✓	HST	×	×	×
[10]	E-TRM, CFD	Constant	×	✓	TOT	✓	Thermography	0.5 °C
[12]	E-TRM	Constant	×	✓	TOT	✓	Mercury Thermometer	0.1 °C
[25]	CFD	Constant	×	✓	HST, TOT	✓	Thermography	HST: N.A. TOT: 0.7 °C
[26]	CFD, AI	Constant	×	✓	HST	✓	OFS	HST: 2 °C
[27]	CFD	Constant	✓	✓	HST	×	×	×
[29]	CFD	Constant	×	✓	HST, TOT	✓	Thermography, OFS	HST: 0.7 °C TOT: 1.0 °C
[30]	CFD	Constant	×	✓	HST, TOT, BOT	✓	N.A.	HST: 4.3 °C TOT: 0.4 °C BOT: 0.8 °C
[31]	CFD	Constant	✓	×	×	✓	Thermography, OFS	×
This Paper	CFD	Accurate Nonuniform	✓	✓	HST, TOT, BOT	✓	Thermography, OFS	HST: 0.1 °C TOT: 0.5 °C BOT: 0.1 °C

Formal analysis, Writing – review & editing, Supervision.

Declaration of Competing Interest

The authors declare that they have no known competing financial interests or personal relationships that could have appeared to influence the work reported in this paper.

Data availability

Data will be made available on request.

Appendix

In Table A1, the complete details and characteristics of the under-studied 500 kVA DT are shown, including tank dimensions, conservator, core, corrugated walls, core, LV and HV windings, and LV and HV oil canals (OCs).

References

[1] IEC 60076-7. Power transformers – "Part 7: Loading guide for mineral-oil-immersed power transformers"; 2018.
[2] IEEE C57.91. IEEE guide for loading mineral-oil-immersed transformers and step-voltage regulators; 2011.
[3] Pradhan MK, Ramu TS. Estimation of the hottest spot temperature (HST) in power transformers considering thermal inhomogeniety of the windings. IEEE Trans Power Deliv 2004;19(4):1704–12.
[4] Taheri AA, Abdali A, Maboudi A, Mazlumi K. Thermal behavior investigation of installation orientation and color effect on distribution transformers using E-TRM method and its effect on loading. Eng Sci Technol Int J 2021;24(2):348–59.
[5] Taheri AA, Abdali A, Taghilou M, Haes Alhelou H, Mazlumi K. Investigation of mineral oil-based nanofluids effect on oil temperature reduction and loading capacity increment of distribution transformers. Energy rep 2021;7:4325–34.
[6] Sun W, Yang L, Zare F, Lin Y, Cheng Z. Improved method for aging assessment of winding hot-spot insulation of transformer based on the 2-FAL concentration in oil. Int J Electr Power Energy Syst 2019;112:191–8.
[7] Novkovic M, Popovic A, Briosso E, Martinez Iglesias R, Radakovic Z. Dynamic thermal model of liquid-immersed shell-type transformers. Int J Electr Power Energy Syst 2022;142(108347):108347.
[8] Sarajcev P, Jakus D, Jolevski D. Transformer insulation coordination using volt–time curve and limit–state surface formulation. Int J Electr Power Energy Syst 2017;90:256–66.
[9] Djamali M, Tenbohlen S. Hundred years of experience in the dynamic thermal modelling of power transformers. IET Gener Transm Distrib 2017;11(11):2731–9.
[10] Shiravand V, Faiz J, Samimi MH, Mehrabi-Kermani M. Prediction of transformer fault in cooling system using combining advanced thermal model and thermography. IET Gener Transm Distrib 2021;15(13):1972–83.
[11] Taheri AA, Abdali A, Rabiee A. A novel model for thermal behavior prediction of oil-immersed distribution transformers with consideration of solar radiation. IEEE trans power deliv 2019;34(4):1634–46.
[12] Taheri AA, Abdali A, Rabiee A. Indoor distribution transformers oil temperature prediction using new electro-thermal resistance model and normal cyclic overloading strategy: an experimental case study. IET Gener Transm Distrib 2020;14(24):5792–803.
[13] Radakovic ZR, Sorgic MS. Basics of detailed thermal-hydraulic model for thermal design of oil power transformers. IEEE trans power deliv 2010;25(2):790–802.
[14] Coddé J, Van der Veken W, Baelmans M. Assessment of a hydraulic network model for zig–zag cooled power transformer windings. Appl Therm Eng 2015;80:220–8.
[15] Swift G, Molinski TS, Lehn W. A fundamental approach to transformer thermal modeling. I. Theory and equivalent circuit. IEEE trans power deliv 2001;16(2):171–5.
[16] Susa D, Nordman H. A simple model for calculating transformer Hot-Spot temperature. IEEE trans power deliv 2009;24(3):1257–65.
[17] Susa D, Lehtonen M, Nordman H. Dynamic thermal modeling of distribution transformers. IEEE trans power deliv 2005;20(3):1919–29.
[18] Tang WH, Wu QH, Richardson ZJ. A simplified transformer thermal model based on thermal-electric analogy. IEEE trans power deliv 2004;19(3):1112–9.
[19] Souza LM, Lemos AP, Caminhas WM, Boaventura WC. Thermal modeling of power transformers using evolving fuzzy systems. Eng Appl Artif Intell 2012;25(5):980–8.
[20] He Q, Si J, Tylavsky DJ. Prediction of top-oil temperature for transformers using neural networks. IEEE trans power deliv 2000;15(4):1205–11.
[21] Chen WG, Su XP, Chen X. Combination of Support Vector Regression with Particle Swarm Optimization for Hot-spot temperature prediction of oil-immersed power transformer. Przeglad Elektrotechniczny 2012;88(8):172–6.
[22] Aizpurua JI, McArthur SDJ, Stewart BG, Lambert B, Cross JG, Catterson VM. Adaptive power transformer lifetime predictions through machine learning and uncertainty modeling in nuclear power plants. IEEE Trans Ind Electron 2019;66(6):4726–37.
[23] Ge Q, Wang M, Jiang YH, Lu YZ, Yao G, Sun C. Health management of dry-type transformer based on broad learning system. IEEE Trans Ind Electron 2021:1.
[24] Mohammed MS, Vural RA. NSGA-II+FEM based loss optimization of three-phase transformer. IEEE Trans Ind Electron 2019;66(9):7417–25.
[25] Raeisian L, Niazmand H, Ebrahimnia-Bajestan E, Werle P. Thermal management of a distribution transformer: An optimization study of the cooling system using CFD and response surface methodology. Int j electr power energy syst 2019;104:443–55.
[26] Deng Y, et al. A method for Hot Spot temperature prediction of a 10 kV oil-immersed transformer. IEEE Access 2019;7:107380–8.
[27] Taghikhani JZ, Taghikhani MA, Gharehpetian GB. Comprehensive comparative analysis of Metal-Oxide nanoadditives impacts on Oil-Filled Finemet and Vitroperm alloy core transformers HST concerning nanofluid thermophysical properties accurate estimation. Energy Convers Manag 2022;260(115594):115594.
[28] Abdali A, Abedi A, Mazlumi K, Rabiee A, Guerrero JM. Precise thermo-fluid dynamics analysis of corrugated wall distribution transformer cooled with mineral oil-based nanofluids: Experimental verification. Appl Therm Eng 2022;no. 119660:119660.
[29] Abdali A, Abedi A, Mazlumi K, Rabiee A, Guerrero JM. Novel hotspot temperature prediction of oil-immersed distribution transformers: An experimental case study. IEEE Trans Ind Electron 2023;70(7):7310–22.
[30] Kebriti R, Hossieni SMH. 3D modeling of winding hot spot temperature in oil-immersed transformers. Electr Eng (Berl, Print) 2022;104(5):3325–38.
[31] Arabul AY, Keskin Arabul F, Senol I. "Experimental thermal investigation of an ONAN distribution transformer by fiber optic sensors", *Electric Power*. Syst Res 2018;155:320–30.
[32] Liu Z, Wang Y, Chen X, Meng X, Liu X, Yao J. An optical fiber sensing method for partial discharge in the HVDC cable system. Int J Electr Power Energy Syst 2021;128(106749):106749.
[33] Guan H, et al. UAV-lidar aids automatic intelligent powerline inspection. Int J Electr Power Energy Syst 2021;130(106987):106987.
[34] Cengel Y, Ghajar A. Heat and mass transfer: Fundamentals and applications. 6th ed. New York, NY: McGraw-Hill Professional; 2019.
[35] Bejan A. Convection Heat Transfer. 4th ed. Chichester, England: John Wiley & Sons; 2013.